

Supersonic Disk Gap Band Parachute Performance in the Wake of a Viking-Type Aeroshell from Mach 2 to 2.5

Anita Sengupta¹

Jet Propulsion Laboratory, California Institute of Technology, Pasadena, CA, 91109

James Roeder², Richard Kelsch³, Mark Wernet⁴
NASA Glenn Research Center, Cleveland, OH, Zip Code, US

and

Walt Machalick⁵, James Reuter⁶, Al Witkowski⁷
Pioneer Aerospace, South Windsor, CT, US

Supersonic wind tunnel testing of 0.813 m diameter Disk-Gap-Band parachutes is being conducted in the NASA Glenn Research Center (GRC) 10'x10' wind-tunnel. The tests are conducted in support of the Mars Science Laboratory Parachute Decelerator System development and qualification. Four percent of full-scale parachutes were constructed similarly to the flight-article in material and construction techniques. The parachutes are attached to a 4% scale MSL entry-vehicle to simulate the free-flight configuration. The parachutes are tested from Mach 2 to 2.5 over a Reynolds number (Re) range of 1 to 3×10^6 , representative of the MSL deployment envelope. Constrained and unconstrained test configurations are investigated to quantify the effects of parachute trim, suspension line interaction, and alignment with the capsule wake. The parachute is constrained horizontally through the vent region, to measure canopy breathing and wake interaction for fixed trim angles of 0 and 10 degrees from the velocity vector. In the unconstrained configuration the parachute is permitted to trim and cone, similar to the free-flight varying its alignment relative to the entry-vehicle wake. Test diagnostics were chosen to quantify parachute performance and to provide insight into the flow field structure. An in-line load cell provided measurement of unsteady and mean drag as a function of Mach and Re. High-speed shadowgraph video of the upstream parachute flow field was used to capture bow-shock motion and stand off distance. Particle image velocimetry of the upstream parachute flow field provides spatially and temporally resolved measurement velocity and turbulent statistics. Multiple high speed video views of targets placed in the interior of the canopy enable photo-grammetric measurement of the fabric motion in time and space from reflective. High speed video is also used to document the supersonic inflation and measure trim angle, projected area, and frequency of area oscillations.

Nomenclature

D_o = Nominal or constructed diameter
 d = Capsule diameter

¹ Senior Engineer, Systems Engineering, 4800 Oak Grove Dr, MS T1723-118, Senior Member.

² Senior Engineer, Department Name, 21000 Brook Park Rd, MS.

³ Senior Engineer, Department Name, 21000 Brook Park Rd.

⁴ Senior Engineer, Department Name, 21000 Brook Park Rd.

⁵ Engineer, 40 S. Satellite Rd., South Windsor, CT Member AIAA.

⁶ Engineer, 40 S. Satellite Rd., South Windsor, CT Member AIAA.

⁷ Chief Engineer, 40 S. Satellite Rd., South Windsor, CT Member AIAA.

- x = Trailing distance defined from capsule maximum diameter to parachute leading edge
- x/d = Non-dimensional trailing distance
- Re = Reynold's number
- M = Mach number
- q = Dynamic pressure
- v = Free stream velocity
- C_D = Drag coefficient
- F_D = Drag
- RMS = Root mean squared
- PIV = Particle image velocimetry
- fps = Frames per second

I. Introduction

THE Mars Science Laboratory spacecraft is scheduled to reach the red planet in 2010. MSL is a robotic exploration mission that will probe the surface of Mars for evidence of organic compounds and continue the search for water. The entry, descent, and landing (EDL) system offers improved landing site access over prior missions including a 10 km surface targeting accuracy, 25 degree ground slope capability, and access to sites up to 2 km above the gravitational equi-potential reference surface¹. This capability enables exploration of previously inaccessible terrain with the potential for enhanced science return. The parachute decelerator system is a critical part of the descent sequence of the MSL entry vehicle. The 21.5-m Disk-Gap-Band (DGB) parachute provides the aerodynamic drag to decelerate the entry vehicle from Mach 2.2 to subsonic speeds, preparing the entry vehicle for powered descent using eight main landing engines. The parachute system expands on the heritage of MPF, MER, Phoenix, Viking, and the pre-Viking era supersonic DGB parachute deployments but also presents a departure from heritage deployment due to its larger size, higher load, and higher Mach deployment relative to the prior Mars deployments².

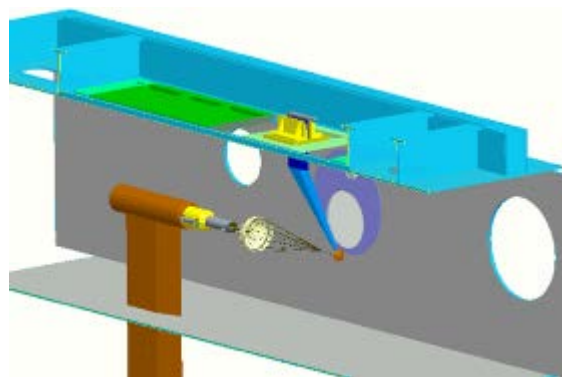


Figure 1. Schematic of the 4% scale MSL supersonic parachute test.

Supersonic wind tunnel testing of 4% scale MSL DGB parachutes is being conducted in support of the MSL parachute development and qualification. The aerodynamic coupling of the entry-vehicle wake to parachute flow-field is under investigation to determine the cause and functional dependence of supersonic canopy localized collapse and re-inflation, characteristic of Viking-type DGB's above Mach 1.5 operation^{3,4,5}. This phenomena, referred to as "area oscillations", leads to large drag oscillations coincident with shape and lateral instability. This instability introduces uncertainties in the modeling of the descent-phase of the mission as well as the potential for dynamics of the capsule under the parachute. Of additional concern to the MSL parachute is the difficulty in quantifying the dynamic loading the parachute will experience due to this instability. The test program was designed to generate a validation dataset for fluid-structure interaction computational tools under development for MSL. It builds from a prior test program and CFD validation effort that utilized a 2.1% scale rigid MSL parachute with capsule to explore the aerodynamic flow field⁶. However

Parameter	GRC	MSL
Nominal Diameter (D_0)	0.813 m	21.5 m
Number of gores	24	80
Capsule / Nominal Diameter	0.21	0.21
Suspension Line Length	$1.7D_0$	$1.7D_0$
Suspension Line Thickness/ D_0	0.0012	0.0002
Max Reynolds number (Re)	1.3×10^6	1×10^6
Max Dynamic Pressure (Pa)	20×10^3	750
Trailing Distance (x/d)	10.6	10.4

Table 1. Comparison of full scale and subscale parachute parameters^{2,5}.

the experimental dataset also provides an empirical understanding of the flow field dependencies and allows an update to the Mach efficiency curve for Viking DGB's, from Mach 2 to 2.5. A comparison of the subscale to full scale parachute is shown in Table 1.

II. Experimental Setup

A. Wind Tunnel Test Configuration

The 4% scale parachute test is being conducted in the NASA Glenn Research Center 10x10 closed-loop Unitary wind tunnel. The test section has a 10x10x40 ft (0.021x0.021x0.85 m) geometry with smooth walls. Mach number is controlled with flexible-wall nozzle geometry that provides Mach 2 to 3.5 operation. The tunnel is calibrated to be within +/- 0.01 Mach and +/-0.25 degree flow angularity. The tunnel operating fluid is air. An exhaust system enables variable pressure operation from 1 to 35 kPa dynamic pressure or 1 to 47 km pressure altitude (on earth). This is equivalent to a Reynolds number range of 3.94×10^5 to $1.12 \times 10^7 / m^7$.

The test configuration is shown in Figure 1. A parachute nominal diameter of 0.813m or 4% scale was chosen to provide the maximum size parachute and to ensure that all capsule shock reflections occur downstream of the parachute. This is needed to preserve the “flight-like” nature of the capsule wake interaction and a precise validation dataset. A swept-back diamond wedge stainless steel strut was selected to mount the 4% scale capsule to. The strut was selected to provide minimum aerodynamic interference with sufficient stiffness to prevent capsule vibration and handle a maximum parachute inflation load of 13.3 kN at a 16° trim angle. Constrained and unconstrained test configurations were investigated to quantify and decouple the effect of parachute trim on coupling to the capsule wake. In both configurations the parachute is attached to the capsule via a load cell as shown in Figure 2 (top). The load cell is hard mounted inside of the capsule. A Kevlar flexible member connects the load cell to a swivel providing the parachute system three rotational and two translational degrees of freedom in the unconstrained condition. The swivel attaches to the parachute single riser. The single riser attaches to the suspension lines through a multi-bridle. The constrained configuration is shown in Figure 2 (bottom). All the textile to metallic component connections were sized to provide the axial trailing distance of $(x/d=10.6)$ defined as the axial distance from the band leading edge to the capsule maximum diameter. The parachute is maintained at a fixed trim angle with respect to the capsule and free stream direction by a constraining rod that goes through the apex of the parachute. It is able to freely translate axially, along a constraining rod, but cannot move radially from the centerline. The parachute hardware that facilitates this motion is discussed later. The constraining rod is attached to the main tunnel mounting stage. In the unconstrained configuration the constraining rod apparatus is removed. The parachute is attached to the capsule as described previously, but is allowed to trim and cone freely in the test section. This configuration is the most representative of the parachute in free flight, however the capsule is at a fixed angle of attack on the strut.

The test matrix is shown in Table 2. The “High q” test conditions were chosen to bound the Mach and Reynolds numbers of the anticipated MSL deployment. Computational fluid dynamics (CFD) analyses suggest that the supersonic parachute instabilities under investigation are turbulence and Mach dependent⁸. For these runs the dynamic pressure in the tunnel is significantly higher than the flight deployment, in order to match the flight Reynolds number at such a small scale. A second set of test conditions, referred to as “Low q”, was chosen for investigation of parachute dynamics at lower Reynolds number (and dynamic pressure) over the same Mach number range. The Low q conditions were selected to increase the lifetime of the test articles needed for the collection of PIV data. They also provide insight into the area oscillation phenomena and parachute drag at lower dynamic pressure for the same Mach number. It is important to note, that at the Low Q runs, the dynamic pressure is 5 to 6 times higher than flight, as the tunnel cannot be pumped down to a lower pressure.

The test-section is equipped with multiple windows for optical access. A pair of 33-in diameter optical grade windows are used for Shadowgraph videography of the flow field around the canopy. Two 20-in windows located

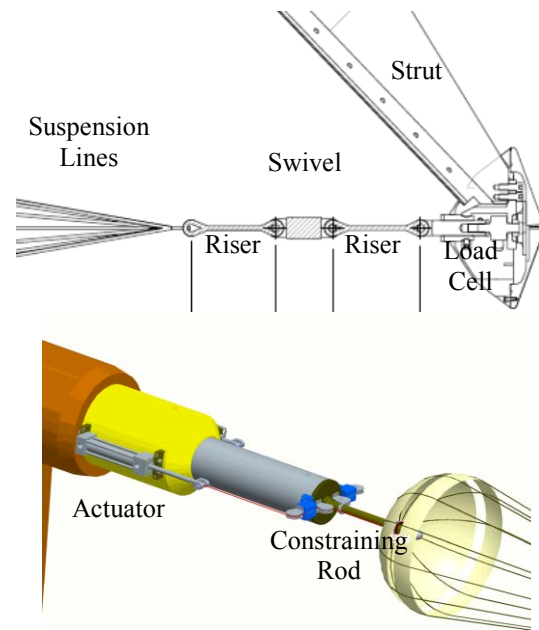


Figure 2. (Top) The capsule to parachute connection. (Bottom) Schematic of the constrained parachute and deployment system.

Test	Mach	High Q		Low Q		Trim (deg)	d/D _o	D _o (m)	x/d
		Re (x10 ⁶)	q (kPa)	Re (x10 ⁵)	q (kPa)				
Constrained	2	0.77	17.4	2.0	4.3	0	0.21	0.813	10.6
	2.2	1.03	18.6	2.4	3.8				
	2.5	1.29	19.9	2.5	3.1				
Constrained	2	0.77	17.4	2.0	4.3	10	0.21	0.813	10.6
	2.2	1.03	18.6	2.4	3.8				
	2.5	1.29	19.9	2.5	3.1				
Unconstrained	2	0.77	17.4	2.0	4.3	variable	0.21	0.813	10.6
	2.2	1.03	18.6	2.4	3.8				
	2.5	1.29	19.9	2.5	3.1				

Table 2. 4% scale DGB parachute-with-capsule test matrix⁶.

just above the Schlieren windows are used for PIV cameras. The PIV laser sheet is fed through a 10-in window in the tunnel test section floor providing a stream-wise plane upstream of the parachute from an x/d of 6 to 10. Two 33-in windows upstream of the capsule are used for high speed video cameras and lighting. Two additional windows in the floor and ceiling, also upstream of the capsule, provide high speed video footage from the floor and ceiling⁶.

B. Subscale Parachutes

The subscale test articles are 4% of the full scale parachute (Figure 3). Table 1 documents the properties of these test articles. They are 0.813 m in nominal diameter with zero porosity Nylon broadloom and forty Kevlar suspension lines. The Kevlar suspension lines connect to a multi-bridle assembly that connects to a Kevlar single riser. The parachutes are geometrically scaled from the standard Viking configuration yielding identical vent area, band height, geometric porosity, etc. They are not identical from a material properties perspective, due to the higher dynamic pressure environment needed to match the flight Reynolds number in the wind tunnel environment. The high dynamics pressure deployment necessitates the use of 1.15 oz/yd² Nylon and proportionately thicker than flight scale suspension lines. The material scaling differences increase the stiffness of the subscale articles relative to full-scale. The inflated shaped may also differ in the band leading edge region, but the effect on the parachute's response is believed to be second order. Proportionately thicker suspension lines have the most significant effect by increasing geometric blockage in the vent region and in generation of shocks and subsonic wake structure. This will be discussed in more detail in section IV.

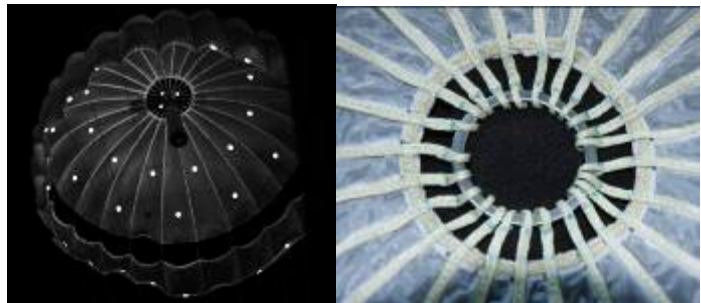


Figure 3. Images of the 4% scale parachute. (Left) View inside the fully open canopy at Mach 2.2, (right) apex region of the constrained parachute showing metallic vent ring.



Figure 4. Constrained parachute rigged in the deployment sleeve. (Top) View showing rip cord and lazy leg. (Bottom) View showing bungee and break cord.

The constrained parachutes have the added feature of a stainless steel vent ring in the apex of the canopy allowing a trim angle relative to the free-stream axis. Figure 3 (right) is an image of the vent region of the parachute. Each vent line terminates at the ring and a two-piece bushing is placed around the ring. The bushing has a smooth bore interior allowing minimal frictional resistance as the parachute travels on the constraining rod. The constraining rod was sized to allow for free upstream and downstream translation of the parachute. The bushing and rod are shown in the rigged configuration in Figure 4. A hemispherical end cap is placed on the end of the restraining rod, to prevent the parachute from coming off of the rod. The geometric vent blockage of the rod and vent ring was accommodated by increasing the constrained parachute vent diameter. The vent open area was scaled to the Viking configuration.

Deployment of the parachutes in supersonic flow was a significant challenge in the design of these tests. Specifically, the subsonic startup environment of the wind tunnel is characterized by highly turbulent and separated flow. It was determined that the parachutes would not survive the required 30 minutes, in this flow environment, prior to getting on condition as the tunnel compressors come online. This necessitated a deployment mechanism to protect the parachute prior to the tunnel reaching condition. The deployment method selected was a Spectra deployment sleeve that would unlace by means of a break-tied daisy chain cord actuated on command. The sleeve was designed to unlace from apex to leading edge, ensuring separation of the sleeve prior to the onset of parachute inflation and preventing friction burning. Sleeve deployment was triggered by a hydraulic actuator that broke a break line to which a rip cord was attached. The rip cord was secured to the sleeve via Teflon pull pins that were inserted through Spectra loops on either side of the sleeve seam. The termination of the rip cord was a pull pin that closed off the mouth of the parachute (Figure 4). A bungee loop was used to provide sufficient force and stroke distance to pull the rip cord after the break cord was broken by the actuator. The bungee was tensioned by the same actuator as the break cord. A lazy leg was also attached to the downstream end of the sleeve and to the bungee, and was sized such that following removal of the rip cord the remaining bungee force would pull on the lazy leg, causing it to pull the sleeve away from the canopy and thereby eliminate any potential interaction between the inflating parachute and sleeve.

C. Diagnostics

Non-intrusive diagnostics were chosen to minimize interference with the wake structure and its interaction with the parachute flow field. Shadowgraph of the canopy bow shock region was obtained through 33-in optical windows on either side of the test article (Figure 1). Images were collected at 2000 to 4000 fps allowing resolution of the frequency and morphology of the parachute bow shock oscillation. The data yields shape and standoff distance measurements for comparison to CFD predictions.

Drag was measured with a single axis load cell mounted within the capsule. Force was measured from the parachute single riser through the swivel in the free stream flow direction. Data was collected at 10 kHz. Drag is calculated in the same method as the Viking era wind tunnel programs for consistency.

$$C_D = \frac{F_D}{q \frac{1}{4} \pi D_o^2}$$

High speed pressure transducers and static pressure ports were also placed on the capsule back shell to provide pressures of mean and RMS pressure at a known point locations. These transducers use the reference static ports to define the absolute pressure.

High speed video data was collected for both imaging and photogrammetric measurement purposes. A total of 4 camera views were used: left side, right side, top, and bottom, all focused on the canopy. The cameras were operated from 1000 to 4000 fps depending on the needed data output. Subsequent testing revealed 2000 fps was needed to resolve the canopy motion post-inflation for the photogrammetric post-processing technique.

Particle image velocimetry (PIV) was used to measure the three components of velocity in the parachute bow shock region equivalent to an axial plane centered in the tunnel, from the $x/d=6$ to $x/d=10$ position. Figure 5 shows the PIV configuration and location of the laser light sheet relative to the parachute and capsule. PIV images were recorded at 3Hz for 5 to 10 minutes providing 900 to 1800 instantaneous measurements of the velocity field in this



Figure 5. PIV data plane in the tunnel. The flow direction is from right to left.

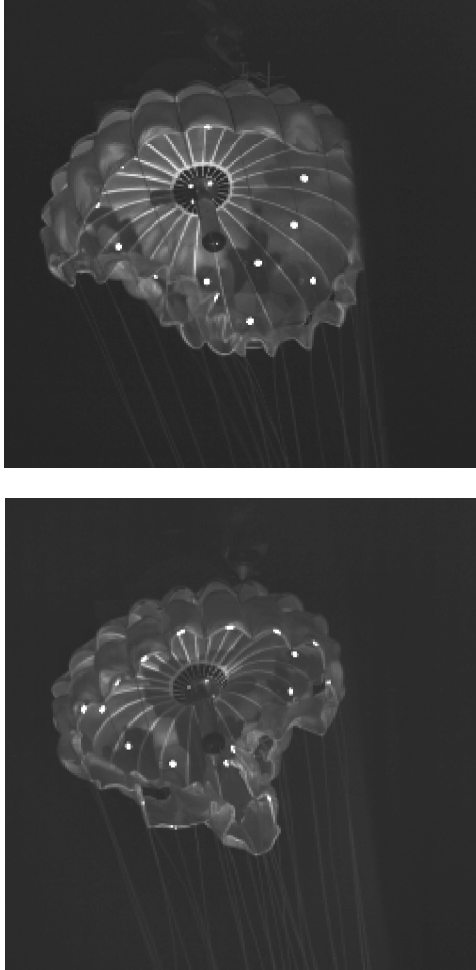


Figure 6. Area oscillation at (top) Mach 2.2 and (bottom) Mach 2.5 for the 0 degree constrained configuration.

variation was observed to increase with Mach number from 2 to 2.5. Projected area ranged from 46% to 68% of full open during an oscillation event from Mach 2 to 2.5 respectively. It is important to note that the onset of an oscillation appeared to be random, however once an oscillation occurred it was followed by 2 to 3 subsequent collapses and re-inflations that did follow a prescribed period. The frequency associated with the oscillations was between 70 and 90 Hz for Mach 2.0 to 2.5. The onset of an oscillation event may be related to suspension line interaction. As will be discussed in section IV, suspension line shocks were seen to disrupt the bow shock in the Shadowgraph high speed video. Another observation was made from the low dynamic pressure runs. The low q runs experienced less violent projected area fluctuations than their high q counterparts for the same Mach number, illustrating the turbulence dependency of the phenomenon.

region. The data yields mean 3 component velocity, 3-component RMS velocity, and turbulence statistics. The data also yields mean and RMS bow shock shape and stand-off distance and frequency of its motion. Knowledge of the time stamp of each instantaneous measurement also allows reconstruction of periodic motions⁹.

III. Experimental Results

Experimental results documented below include description of the canopy motion and fabric dynamics from high speed video, as well as drag and shadowgraph of the parachute flow field. Photogrammetric and PIV data reduction is underway and will be presented in a future publication. Only results from the 0 degree constrained configuration are presented. The 10 degree and unconstrained configuration experimental dataset is not yet complete.

A. Parachute Dynamics

Figure 3 (left) shows the fully inflated canopy in its representative at Mach 2.2 operation. The parachute fabric dynamics were predominantly periodic in-folds of the band region with their frequency and deflection increasing with Mach number from 2.0 to 2.5. Area oscillations, as previously observed in the Viking and pre-Viking supersonic test programs, did occur at all three Mach numbers investigated. Area oscillation events are shown in Figure 6. The collapse event propagates from the band leading edge inward towards the center of the canopy. The area oscillations can be characterized by the maximum projected area reduction experienced and the frequency or period associated with the collapse and subsequent re-inflation. Projected area

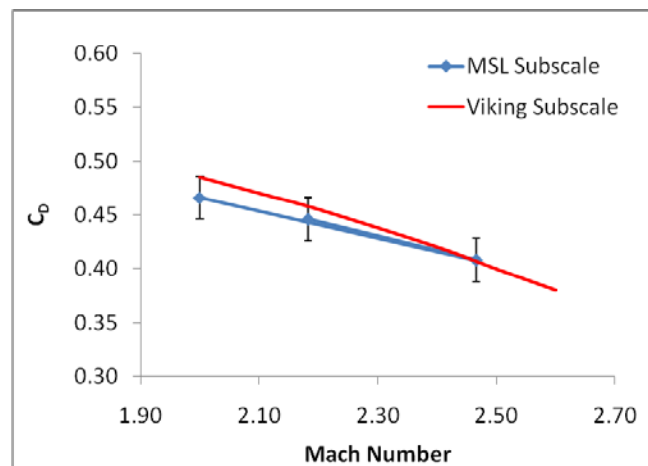


Figure 7. Measured drag coefficient for the MSL subscale of 0-deg constrained plotted with Viking subscale drag coefficient measurements [Error!

B. Drag Performance

The measured drag coefficient versus Mach number is plotted in Figure 7 for the high Q runs only. The data is plotted against the data obtained in the pre-Viking supersonic wind tunnel program¹⁰. The trend to decreasing C_D with Mach number is evident in the zero degree constrained dataset. The measurements compare well with the Viking subscale data set over the same Mach number range. It should be noted that the Viking data was from unconstrained parachutes with an $x/d=8.5$. Although not shown, the RMS component of the drag also increased with Mach number from 2 to 2.5. The initial inflation drag profile did follow an exponential trend, similar to full scale supersonic inflations. A frequency content analysis has not yet been performed.

C. Shadowgraph

The shadowgraph data revealed the pressurization and depressurization of the parachute was driven by the changing morphology and standoff distance of the parachute bow shock (Figure 8). The cyclical motion was similar to that of the rigid parachute experiments described in reference [6] confirming that the fundamental physical mechanisms driving the parachute instability are aerodynamic in nature. As will be discussed in the next section, a critical finding is that suspension line shock generation seems to exacerbate the canopy instability by disrupting the parachute bow shock completely in some instances. Frequencies of bow shock oscillation are consistent with the acoustic frequency, i.e. the time constant for a fluid particle to travel from the parachute to capsule.

Other interesting features in the Shadowgraph data include an asymmetric bow shock, which can be attributed to the strut contribution to the wake, and a secondary pressure discontinuity or contact surface at the canopy mouth.

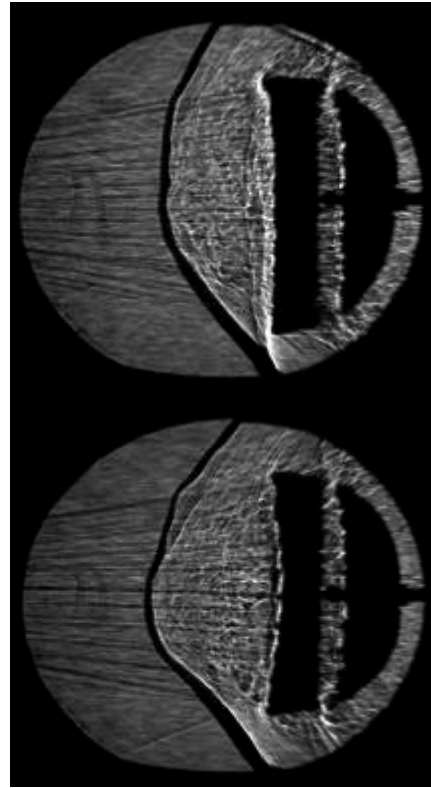


Figure 8. Shadowgraph of parachute bow shock at (top) Mach 2.2 and (bottom) Mach 2.5 for the 0 degree constrained configuration.

IV. Discussion

A. Mach and Re Dependence

There is a well documented Mach dependence to all parameters that were measured from Mach 2 to 2.5. Drag coefficient decreases with Mach number from 2 to 2.5. Qualitatively, the parachute lateral and inflation stability was affected by the increasing Mach number. Mach 2.5 was the most unstable of the three mach numbers investigated. Shadowgraph data supports this trend as well. The parachute bow shock morphology was more chaotic with increasing mach and the parachute canopy fabric responded in kind. Reduced drag and increase lateral instability negatively impacts effects EDL performance. Mean drag variation can be captured in the Mach efficiency curve, but dynamic stability coefficients are not yet defined for Mars parachute use. From a structural perspective, a more dynamic flow environment stresses the canopy fabric and may increase the abrasive loading in highly loaded textile members.

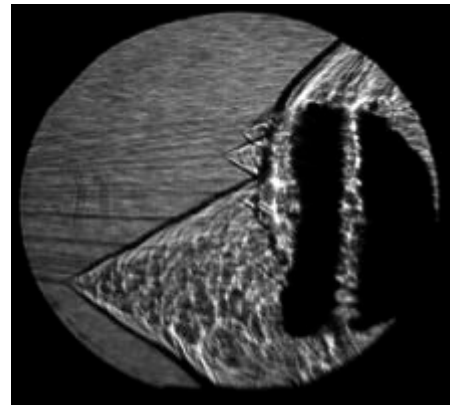


Figure 9. Area Oscillation at (left)Mach 2.2 and (right)Mach 2.5 for the unconstrained configuration.

B. Suspension Line Interaction

Table 1 lists the ratio of suspension line thickness to parachute nominal diameter for the full scale and 4% scale parachute. The subscale parachute lines are 6.5 times thicker and occupy 47

times the area as compared to the full scale article. Therefore any suspension line effects will be exacerbated in the subscale test as compared to actual flight. Figure 10 is an image of the bow shock region of the parachute during an unconstrained run to illustrate this effect. Shocks from the suspension lines create large density disturbances that at times disrupt the parachute bow shock in the Shadowgraph video. The response of the parachute to this disruption was oscillatory motion of the canopy, i.e. an area oscillation. The suspension line shocks therefore exacerbate canopy breathing. This is also very important because the original Viking parachutes used Dacron suspension lines with a thickness to nominal diameter ratio of 0.00157, similar to that of the MSL subscale test article¹⁰. We can expect this effect to be reduced for the full scale flight. As such, the non-dimensionalized number, frequency and magnitude of area oscillations in the subscale test should be a conservative representation of the flight supersonic

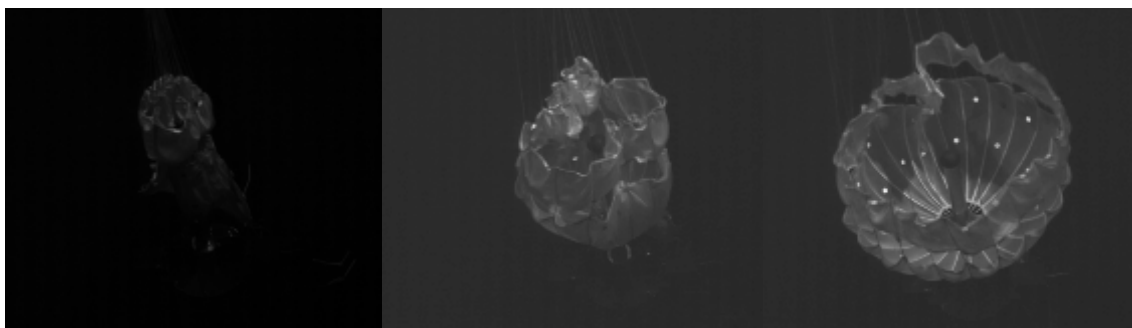


Figure 10. Images of supersonic initial inflation at Mach 2.5 for the 0-deg constrained case. The images document, left to right, 2, 4, and 5.5 ms from sleeve release (deployment).

environment.

C. Supersonic Inflation

High speed video and shadowgraph of the initial inflation was also obtained. Inflation time in this test program is defined as sleeve release to first full open. It ranged from 7.5 to 14 ms for the 0-degree configuration. Although different from a mortar deployment, due to the absence of bag striping forces/tensioning, the test configuration does provide insight into the aerodynamics at line stretch and how the canopy band and disk behave in a supersonic environment post bag strip. Figure 10 shows the parachute from 2 to 5.5 ms into its initial supersonic inflation. The parachute unfurls from its flaked configuration in an orderly fashion. At 4 ms into the inflation the canopy presentation is similar to that during an area oscillation event. It should be noted that no flag drag or flapping dynamics were observed during the inflation. The supersonic fill time constant is quite short, preventing these common subsonic modes from ever appearing prior to a fully inflated condition.

V. Conclusion

A series of wind tunnel experiments were performed to determine the supersonic performance of a subscale representation of the MSL DGB parachute in the wake of a Viking-type biconic aeroshell. The Mach and Reynolds number dependence of the parachute's performance was investigated and quantified with non-intrusive diagnostic techniques. Shadowgraph in conjunction with high speed video revealed that canopy fabric dynamics are caused by variations in the shape and standoff distance of the parachute bow shock. The magnitude and frequency of this variation was a function of Mach number, Reynolds number, and suspension line interaction. The changing shape corresponded to pressurization and depressurization of the canopy resulting in periodic fabric motion and in some instances large projected area fluctuations. The majority of the canopy motion was band oscillation with leading edge infolds. However, the supersonic instability referred to as area oscillations were observed and documented with Shadowgraph and high speed video. They occur when the bow shock is disrupted, and were more prevalent with increasing the Mach number and Reynolds number. A critical finding is the effect suspension line shocks have on the canopy stability. Area oscillations tended to be augmented by suspension line interaction with the conical shock. Supersonic inflation video did not reveal any usual motion or behavior of the canopy and occurred in less than 15 ms. The parachute appeared to inflate from the mouth and followed an orderly unfurling defined by its flaked condition from rigging

In summary the parachute drag performance is consistent with prior Viking DGB parachutes tested in this regime. The Mach efficiency curve for MSL will be updated to include the measured drag coefficient in the 2.0 to

2.5 range. The area oscillation frequency and dynamics are less severe than previously thought and the physics that drive them consistent with CFD simulations of a rigid parachute configuration.

Acknowledgments

The authors would like to acknowledge Al Linne, Dan Kovach, Gary Huber, Matt Organzally, Mark Woike, Christine Pastore, Lance Foster, Dave Stark, Roland Gregg, and Joe Rossoll from NASA GRC; Dutch Slager, Adam Steltzner and Keith Comeaux from the Jet Propulsion Laboratory; Graham Candler from the University of Minnesota; Carlos Pantano from the University of Illinois; and Mike Kandis and Anthony Levay from Pioneer Aerospace Corporation. The Jet Propulsion Laboratory, California Institute of Technology carried out these activities under a contract with the National Aeronautics and Space Administration.

References

-
- ¹ D. Way, R. Powell, A. Chen, and A. Steltzner, "Asymptotic Parachute Performance Sensitivity" 2006 IEEE Aerospace Conference, Big Sky, MT, March 2006.
 - ² A. Sengupta, A. Steltzner, A. Witkowski, and J. Rowan, "An Overview of the Mars Science Laboratory Parachute Decelerator System," IEEE-1432-2007, March 2007.
 - ³ H. Murrow and J. Mcfall, "Some Test Results from the NASA Planetary Entry Parachute Program," *J. Spacecraft*, Vol. 6 (5): 621-623, 1969.
 - ⁴ D.E Reichenau., "Aerodynamic Characteristics of Disk-Gap-Band Parachutes in the Wake of Viking Entry Forebodies at Mach Numbers from 0.2 to 2.6," AEDC-TR-72-78, Arnold AFB, Tennessee, (1972).
 - ⁵ D. Dickenson et. al., "Balloon Launched Decelerator Test Post-Flight Test Report BLDT Vehicle AV1," TR-3720289, Sept 1972.
 - ⁶ A. Sengupta et. al., "Results from the Mars Science Laboratory Parachute Decelerator System Supersonic Qualification Program," IEEE-1435-2008, March 2008.
 - ⁷ <http://facilities.grc.nasa.gov/documents/TOPS/Top10x10.pdf> , "10- by 10-Foot Supersonic Wind Tunnel," TOP3-00226, Jan 2007.
 - ⁸ M. Barnhardt, T. Drayna, Ioannis Nompelis, G.V. Candler, and W. Garrard, "Detached Eddy Simulations of the MSL Parachute at Supersonic Conditions," AIAA-2529-2007, May 2007.
 - ⁹ A. Sengupta et. al, "Supersonic Qualification Program for the Mars Science Laboratory Parachute Decelerator System," AIAA 2007-2542, May 2007
 - ¹⁰ I. Jaremenko, S. Steinberg, and R. Faye-Petersen, "Scale Model Test Results of the Viking Parachute System at Mach Numbers from 0.1 Through 2.6," TR-3720181, November 1971.